

# The spectral variability of the cool hypergiant $\rho$ Cassiopeiae<sup>\*</sup>

A. Lobel<sup>1\*\*</sup>, G. Israelian<sup>1,2,4</sup>, C. de Jager<sup>3</sup>, F. Musae<sup>5</sup>, J.Wm. Parker<sup>6</sup>, and A. Mavrogiorgou<sup>1</sup>

<sup>1</sup> Astronomy Group, Vrije Universiteit Brussel, Pleinlaan 2, B-1050 Brussels, Belgium

<sup>2</sup> Chatterton Astronomy Department and RCfTA, School of Physics A28, University of Sydney, 2006 NSW, Australia

<sup>3</sup> SRON Laboratory for Space Research, Sorbonnelaan 2, 3584 CA Utrecht, The Netherlands

<sup>4</sup> Instituto de Astrofísica de Canarias, E-38200 La Laguna, Tenerife, Canary Islands, Spain

<sup>5</sup> Special Astrophysical Observatory, Russian Academy of Sciences, Nizhnii Arkhyz, Stavropol'skii Kraii, 357147, Russia

<sup>6</sup> Southwest Research Institute, Suite 429, 1050 Walnut Street, Boulder, CO 80302, USA

Received 30 January 1997 / Accepted 12 August 1997

**Abstract.** We checked the change of the effective temperature with the atmospheric pulsation of  $\rho$  Cas from combined analyses of optical spectra of 1993-95 and *IUE* spectra of 1979-81. We find an upper range for  $\Delta T_{\text{eff}} \simeq 750$  K over a period of 16-17 months. We present a thorough study of the related absorption line profile changes from which a velocity stratification with excitation energy could not be detected for the metallic lines. The distinct evolution of  $H\alpha$  displays variable distortions of filling-in by emission with the pulsation. Our theoretical line profile fits yield a value for  $v \sin i$  of  $25 \text{ km s}^{-1}$ .

We report the finding of two different causes for the splitting of absorption line cores in the spectra of  $\rho$  Cas. For the phase near highest effective temperature we have analyzed the development of very far shortward extended line wings assuming velocities up to  $150 \text{ km s}^{-1}$ . These violet absorptions originate about  $2.5 R_*$  above the photosphere in a cool and variable supersonic wind from which we determine an upper value of the mass-loss rate of  $9.2 \cdot 10^{-5} M_{\odot} \text{ y}^{-1}$ . We also report the finding of an increase of the supersonic wind velocity by  $\sim 15 \text{ km s}^{-1}$  per electronvolt decrease, measured from the maximum velocities of these violet absorptions for Fe I lines.

A separate analysis of the *IUE* spectra reveals tremendous changes of the Balmer continuum flux by a factor 4 to 5 in only 26 hours, clearly distinct from the long-term variations of  $H\alpha$ .

**Key words:** stars: oscillations; variables; atmospheres; supergiants;  $\rho$  Cas – line: identification – line: profiles

---

Send offprint requests to: A. Lobel (alexl@ster1.vub.ac.be)

\* Partly based on observations taken at the La Palma Observatory, the Special Astrophysical Observatory and with the International Ultraviolet Explorer

\*\* Research Assistant of the Fund for Scientific Research - Flanders (Belgium)

## 1. Introduction

$\rho$  Cas can be considered as the prototype object of the yellow hypergiants. These cool luminous stars are found in the Hertzsprung-Russell diagram close to their limit of existence, showing spectral and photometric variability with quasi-periods ranging to several years.

The atmospheric structure of F- and G-type supergiants is very complex. These extended atmospheres are complicated by varying dynamical perturbations like acoustic and gravity waves and the poor knowledge of their influence on the atmospheric structure and the resulting stellar spectrum. Also the influence of atmospheric sphericity effects and the presence of supersonic microturbulent velocity fields is hardly understood. For an overview and discussion of many of these topics for the most luminous supergiants we refer to de Jager (1980).

The spectral monitoring of  $\rho$  Cas is recommended because there are no indications of binarity for this bright supergiant. The binarity of HR8752 severely complicates the spectral analyses of this bright spectral twin of  $\rho$  Cas. The majority of the other known yellow hypergiants is much fainter for which it is less simple to reduce the spectral noise and thus to define the local continuum level in the optical.

A study of the combined spectral and photometric variability of  $\rho$  Cas covering about half the photometric pulsation period of 1970 has recently been given in Lobel et al. (1994). In the present paper we extend the investigation of these spectral changes in the optical by means of nine spectra obtained between Nov. '93 and Dec. '95. The aim of this analysis is to check the range of the effective temperature change with the pulsation of the atmosphere. To that end a detailed study of absorption line profile changes is required. This study is combined with an analysis of the *IUE* spectra obtained in 1979-81. Besides an investigation of possible stratification effects previously reported in the extended atmosphere of  $\rho$  Cas, we determine the mass-loss rate from optical data in the phase of highest effective temperature,

which we compare to one radio observation in the 6 cm band of March '93.

For the first time we present a study of the structure of the supersonic wind of  $\rho$  Cas which is based on the spectral properties during the phase of highest effective temperature in the pulsation cycle.

## 2. Observations

### 2.1. Optical spectroscopy of 1993-95

We have obtained three high-resolution spectra of  $\rho$  Cas with the Utrecht Echelle Spectrograph (UES) on WHT at La Palma, spanning about 3000 Å in the optical. The spectra have been reduced by utilizing the MIDAS Echelle software package. More detailed information about these spectra obtained in 1993-95 is summarized in Lobel & de Jager (1997).

Five more spectra have been obtained in a monthly service observation program scheduled since June '95 for the Coude Echelle Spectrometer (Musaev 1993) mounted on the 1-m telescope at the Special Astrophysical Observatory (SAO) of the Russian Academy of Sciences. Two of these are of high-resolution with the  $S/N$  ratio exceeding about 100 per bin. The resolution values  $\Delta\lambda$  of the various presently studied data are provided in Table 2. A preliminary reduction procedure of the latter echelle spectra has been carried out with the DECH software package (Galazutdinov 1992).

### 2.2. IUE spectroscopy of 1979-81

The presented UV data is available in the IUE archives. We have reduced the spectra with IUESIPS. After extracting the high-dispersion orders, the echelle-blaze ripple corrections were applied, together with the adjustments of the flux due to the temperature dependent instrument sensitivity. The data are extracted at full resolution without smoothing, which results in a wavelength dependency of  $\Delta\lambda \approx 0.02$  Å at  $\lambda = 1200$  Å to  $\Delta\lambda \approx 0.05$  Å near  $\lambda = 3000$  Å. The absolute flux calibration was performed by utilizing the photometric standards which include TD-1 and OAO-2 stars. The pixel-to-pixel variations and spectral alinearity have been removed by means of intensity transfer functions derived from UV flood-lamp exposures (Nichols & Linsky 1996).

## 3. Variability of the optical spectra of 1993-95

### 3.1. Determination of time-variations of atmospherical model parameters

In Fig. 1 we show the profile changes caused by atmospherical pulsation for three unblended neutral iron lines in the UES spectra. The neutral absorption lines strongly intensify and broaden between Dec. 21 '93 and April 18 '95, which results from the changing atmospherical conditions with time. In this section we present a brief description of the method we have applied to determine the changes of atmospherical model parameters from optical spectra for these two observation dates. This is accomplished by calculating equivalent line width values ( $W_{eq}$ ) by

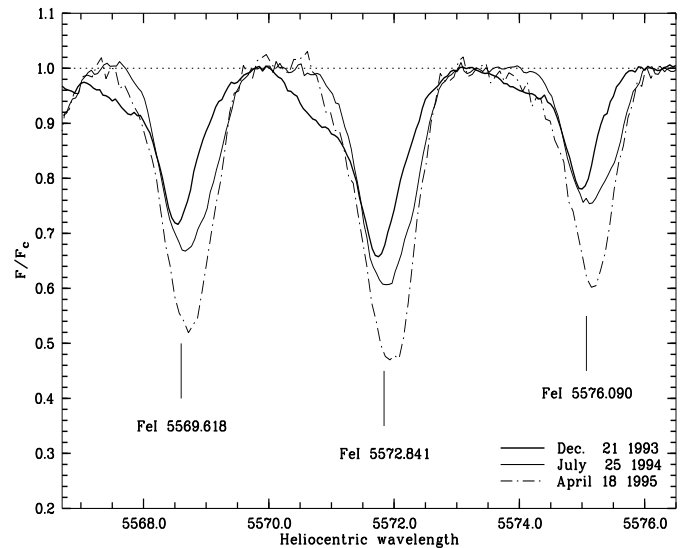


**Fig. 1.** Variability over 16 months of neutral iron lines caused by the atmospherical pulsation of  $\rho$  Cas

means of atmospherical models by demanding that these widths should be as well as possible equal to the observed equivalent widths. The set of chosen model parameters comprises the effective temperature ( $T_{eff}$ ), the effective acceleration of gravity  $\log g_{eff}$ , the logarithmic metallic abundance compared to the solar values  $\Delta \log Z$  and the line-of-sight microturbulence velocity component  $\zeta_{\mu}$ . These quantities are varied and improved iteratively by means of a least-square fit between the computed and observed  $W_{eq}$  values until a 'best' model fit to the lines is derived. A full description of the method can be found in Achmad et al. (1991) and has also been applied and improved for spectra of  $\rho$  Cas of 1970 by Lobel et al. (1994).

A further improvement of the method of spectral diagnostics has presently been carried through by selecting and measuring the observed  $W_{eq}$  values after checking the profiles for hidden absorption line blending. For the tremendously crowded spectra of cool supergiants like  $\rho$  Cas this proved to be required for the further improvement that also compares calculated and observed line profiles beside their  $W_{eq}$  values. To achieve this goal we have computed theoretical-synthetic spectra over the whole optical wavelength range covered by our data using the grid of Kurucz (1991) atmospherical models between 4500 K and 7500 K with lowest  $\log g$ . This method, combined with a multi-gaussian technique retained 23 Fe I and 11 Fe II lines for which we have measured the  $W_{eq}$  and FWHM value.

In Fig. 2 we have plotted the observed FWHM values against  $W_{eq}$  covered by Table 1 for the three UES spectra of 1993-95. Since we have measured the  $W_{eq}$  values by integrating the optimal gaussian fit to the observed profile, these two quantities are linked by:  $FWHM = 2 W_{eq} / (I_0 \sqrt{\pi})$ , where  $I_0$  is the central line depression. Fig. 2 shows that the weakest lines have FWHM values already exceeding 400 mÅ and the profiles broaden almost linearly with ascending  $W_{eq}$ . The slope of a linear fit to the

**Table 1.** Observed equivalent widths and FWHM values of iron lines for three UES spectra. Computed equivalent widths are given for the best atmospherical model fit. Column 5 is given for  $\Delta\log Z$  set to solar abundance instead of 0.3 in column 4 (see text)

Obs. date	Dec. 21 '93				July 25 '94			April 18 '95			$\log(gf)$	$\chi_{\text{low}}$ (eV)	Mult.
No.	$\lambda_0$ (Å)	$W_{\text{eq}}^{\text{obs}}$	$W_{\text{eq}}^{\text{cal}}$	$W_{\text{eq}}^{\text{cal}}$	FWHM	$W_{\text{eq}}^{\text{obs}}$ (mÅ)	FWHM	$W_{\text{eq}}^{\text{obs}}$	$W_{\text{eq}}^{\text{cal}}$	FWHM			
$\Delta\log Z$		0.3	0.0						0.3				
Fe I													
01	4903.316	365	294	150	979	384	754	454	473	721	-0.930	2.882	(318)
02	4966.095	318	198	086	878	316	820	437	378	806	-0.870	3.332	(687)
03	4973.101	138	072	026	677	211	874	315	183	920	-0.950	3.960	(984)
04	5049.827	296	312	162	610	659	1017	617	507	881	-1.360	2.279	(114)
05	5090.79	092	-	-	522	590	703	145	-	560	-0.400	4.256	(1090)
06	5126.192	092	-	-	507	-	-	015	-	223	-1.080	4.256	(1089)
07	5133.699	232	197	108	629	327	876	326	279	713	+0.140	4.178	(1092)
08	5159.050	092	056	020	637	121	704	177	146	592	-0.820	4.283	(1091)
09	5281.798	140	289	145	564	380	929	498	471	956	-0.830	3.038	(383)
10	5329.987	063	019	007	713	-	-	107	054	552	-1.220	4.076	(1028)
11	5364.858	250	276	144	788	336	970	438	399	918	+0.294	4.446	(1146)
12	5367.476	226	345	196	726	300	895	311	484	731	+0.440	4.415	(1146)
13	5383.380	246	281	196	746	339	910	382	354	846	+0.640	4.312	(1146)
14	5389.46	066	103	039	461	126	806	198	228	742	-0.410	4.415	(1145)
15	5393.17	219	213	094	812	307	962	363	397	847	-0.910	3.241	(553)
16	5400.51	110	165	069	553	183	846	226	305	705	-0.160	4.371	(1145)
17	5415.192	261	406	269	692	252	704	363	516	703	+0.669	4.386	(1165)
18	5569.618	260	187	097	856	333	941	467	286	904	-0.540	3.417	(686)
19	5572.841	330	301	184	932	417	981	545	406	956	-0.310	3.396	(686)
20	5576.090	144	146	058	633	236	886	355	316	841	-1.000	3.430	(686)
21	5633.975	080	087	032	676	107	842	104	190	597	-0.060	4.991	(1314)
22	5686.53	067	095	035	639	139	1011	227	213	876	-0.360	4.549	(1182)
23	5862.368	100	112	043	727	113	1116	123	240	703	-0.270	4.549	(1180)
Fe II													
01	4893.817	271	194	087	797	313	871	341	314	841	-4.450	2.828	(36)
02	5018.450	-	944	872	-	-	-	962	999	1225	-1.220	2.891	(42)
03	5061.718	-	048	019	-	-	-	051	039	597	+0.217	10.308	
04	5120.352	251	269	130	764	247	819	245	398	768	-4.214	2.828	(35)
05	5316.620	-	815	718	-	790	1042	670	887	919	-1.850	3.153	(49)
06	5325.553	541	497	423	1090	377	809	366	552	762	-2.600	3.221	(49)
07	5362.867	-	570	439	-	590	893	504	664	779	-2.920	3.199	(48)
08	5414.075	443	321	164	977	469	1172	398	455	855	-3.790	3.221	(48)
09	5425.259	452	296	206	938	410	850	378	353	747	-3.360	3.199	(49)
10	5525.125	-	080	029	-	353	1179	347	156	979	-4.609	3.267	(56)
11	5567.842	-	092	035	-	067	701	114	114	606	-1.887	6.730	

Fe I data (triangles) of Dec. 21 '93 declines from 0.95 to 0.71 in April 18 '95, which indicates an overall increment of the core depression in the latter spectrum.

For the theoretical line profile modeling we have utilized the SYNSPEC code (Hubeny, priv. comm.). It solves the radiative transfer for the atomic parameters given in Table 1. The micro-turbulent velocity is treated as an additional term to the thermal broadening, as is computed from the temperature in the selected atmospherical model. For details about the considered opacity sources and other atomic broadening mechanisms we refer to the CCP7 library on Internet (<http://star.arm.ac.uk/ccp7>).

The first iterations aimed to fix the  $\Delta\log Z$  parameter. This was achieved by noting that models with solar abundance val-

ues directed the iteration path toward very low  $T_{\text{eff}}$  values below 4000 K, which is excluded for the spectral character of  $\rho$  Cas (F8 Ia<sup>+</sup>). The best correspondence with the observed  $W_{\text{eq}}$  was obtained for  $\Delta\log Z=0.3$ , which confirms the value of +0.39 obtained for the spectra of 1970. Our final iteration, by keeping  $\Delta\log Z$  fixed at 0.3, yields for the data of April 18 '95 the best model parameters ( $T_{\text{eff}}=6500$  K,  $\log g=0.5$ ,  $\zeta_{\mu}=12$  km s<sup>-1</sup>). For the data of Dec. 21 '93 we obtain (7250, 1.0, 12). In columns 4 and 10 of Table 1 we list the equivalent widths computed with these models. In column 5 we have added the values computed for  $\Delta\log Z=0.0$  in order to demonstrate the reduction of agreement with the observed values (column 3).

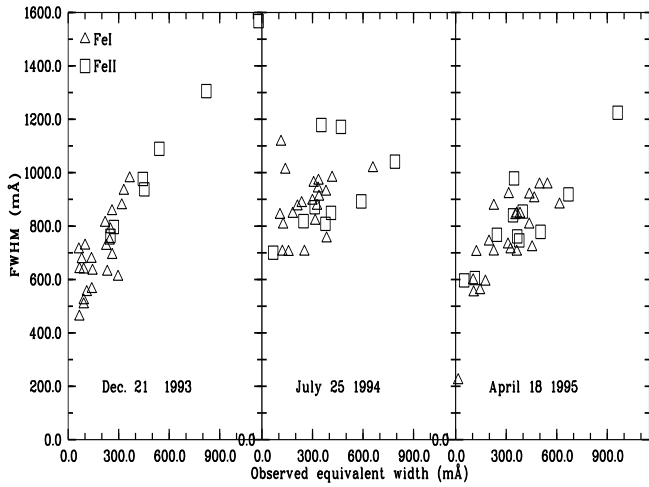


**Fig. 2.** The changes of equivalent width versus FWHM value reflect the variability of the core intensity for 34 unsaturated lines covered by Table 1, selected for the method of spectral diagnostics

In general, the selected models provide a good correspondence with the observed quantities. However, for some lines it remains poor which may be attributed to inaccurate  $\log(gf)$  values. The latter are adopted from Nave et al. (1994) for Fe I, whereas the data for Fe II is taken from Fuhr et al. (1988). In the iteration procedure we required that the difference between the observed and computed values remained below 50 percent. This selection criterion gradually increased the number of retained lines, which results for the final iteration in 26 lines out of 34 for the low temperature phase, and 25 out of 28 lines for the high temperature phase. We found that the calculated  $W_{eq}$  values remained almost unchanged by lowering  $\log g$  for the latter model to 0.5 and which could not improve the agreement with the observed values.

Next to the determination of the best atmospheric model, the observed line profiles are modeled by theoretical profile fits using these models. Hence, we find a  $v \sin i$  value of  $25 \text{ km s}^{-1}$  reproducing the observed line shapes reasonably well. Note that it has to be considered here as an upper value since we presently do not include the line broadening caused by macroturbulent velocity fields. Such rather high rotation velocity for a late-type supergiant like  $\rho$  Cas is however still permitted since the critical break-up velocity is  $\sqrt{GM_*/R_*} \simeq 119 \text{ km s}^{-1}$  for  $M_* = 30 M_\odot$  and  $R_* = 400 R_\odot$  (Lobel et al. 1994). This value for the rotational velocity may still be too large, because, based on an average ZAMS rotational value, one would expect for  $\rho$  Cas a value below  $5 \text{ km s}^{-1}$  (Van den Heuvel 1968). The determination of the macroturbulent velocity field requires an elaborate de-convolution procedure which will be performed on the available spectral sequence in future analyses of  $\rho$  Cas.

In Figs. 3 and 4 we plot the profiles of two unblended Fe I lines at  $5393 \text{ \AA}$  and at  $5576 \text{ \AA}$  observed in the spectrum of Dec. '93 (top) and April '95 (bottom). For comparison we overplot with the theoretical profiles by using the selected models for

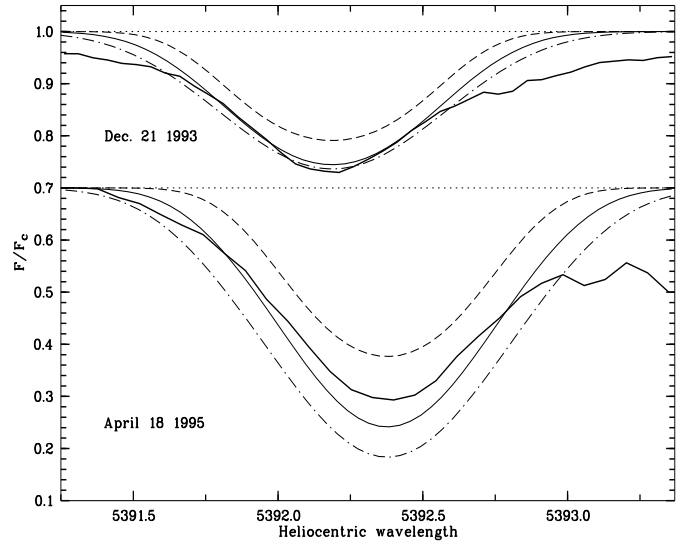


**Fig. 3.** Observed profile of the Fe I line at  $5393 \text{ \AA}$  (thick drawn lines) of Dec. 21 '93 and of April 18 '95 (shifted vertically by 0.3). Thin drawn lines are theoretical profile fits using the best Kurucz model for a turbulent velocity value of  $6 \text{ km s}^{-1}$  (dashed),  $12$  (solid) and  $18$  (dash-dotted). All computed profiles are rotationally broadened by  $25 \text{ km s}^{-1}$

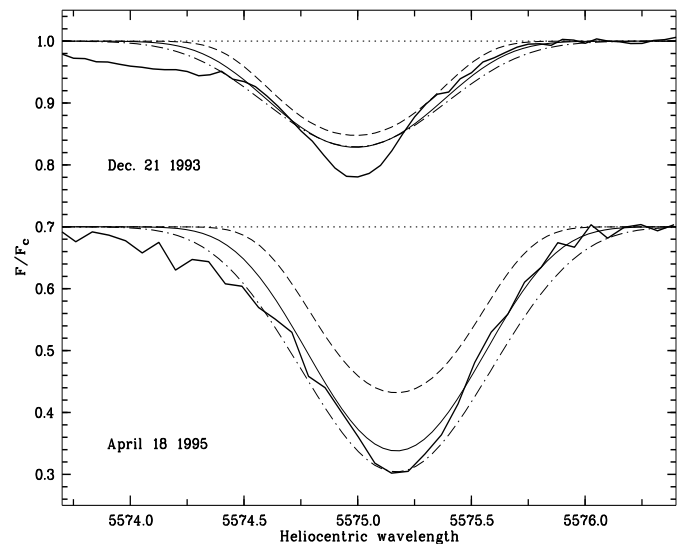


**Fig. 4.** Same as Fig. 3 but for the Fe I line at  $5576 \text{ \AA}$

three different microturbulence values and the rotational broadening fixed to  $25 \text{ km s}^{-1}$ . A least-square fit revealed that these profiles compare best with the observed line shape for  $\zeta_\mu$  between  $10$  and  $13 \text{ km s}^{-1}$ , which we also derived from the model iteration method. Notice that these values are derived for both the low and high  $T_{eff}$  phase. Therefore, the effect from dynamical large-scale motion fields on the derived  $\zeta_\mu$  values (as was discussed by Fokin et al. 1996) remains limited.

**Table 2.** Dates of observation of the optical spectra of 1993-95

Obs. date	No.	JD-2449000+	Inst.	$\lambda / \Delta \lambda$
Nov. 28 1993	1	320	SAO	30000
Dec. 21 1993	2	343	WHT-UES	80000
July 25 1994	3	559	WHT-UES	80000
April 18 1995	4	826	WHT-UES	80000
June 09 1995	5	878	SAO	36000
July 31 1995	6	930	SAO	80000
Sept. 06 1995	7	967	SAO	80000
Oct. 13 1995	8	1004	SAO	36000
Dec. 03 1995	9	1055	SAO	36000

### 3.2. Spectral monitoring since Nov. 1993

A monthly spectral monitoring program for  $\rho$  Cas is presently scheduled at SAO. We intend to cover at least one complete spectral pulsation period in order to determine the changes of the atmospheric model parameters and to compare the spectral and photometric periodicity, when sufficient photometrical data becomes available. The dates of spectral observations are given Table 2.

Fig. 5 shows the evolution of the Fe I 5572.841 Å line covering a period of two years. We have checked from theoretical-synthetic spectrum calculations that the profile is free from hidden line blending by weak absorption lines in the wings. The continuum level is therefore reliably defined, within an accuracy of a few percent at most. The velocity scale is heliocentric and the dotted vertical line is drawn at the center-of-mass velocity. The latter has been measured from a forbidden [Ca II] emission line emerging from the cool tenuous envelope which surrounds  $\rho$  Cas (Lobel & de Jager 1997). The iron line displays three main properties with its evolution, which are also observed in other metallic absorption lines having relatively high excitation energies ( $\chi_{\text{low}}$  exceeding 3 eV).

1. the line intensifies when broadening in the time-sequence and narrows by weakening.
2. the broadening of the line occurs mainly at the long wavelength side of the core profile and, after having reached maximum redward extension (July-Sept. '95) it also narrows from that side. The short wavelength side of the core profile remains almost static.
3. when the line core assumes maximum depression the profile becomes nearly symmetric and centers around the systemic velocity (in the phase of minimum  $T_{\text{eff}}$ ), whereas the lines become weakest showing a rather triangular profile shape where the line bisector appears blue-shifted with respect to the systemic velocity (the phase of maximum  $T_{\text{eff}}$ ).

The grayscale representation of this Fe I line is shown in the right panel of Fig. 6. The velocity scale ranges from -150 km s<sup>-1</sup> to 50 km s<sup>-1</sup>. Time runs upward and the five upper strips are the recent SAO observations, collected monthly since June '95. This sequence, together with the UES spectrum of April '95 (strip 4) reflects subsequent atmospheric changes within

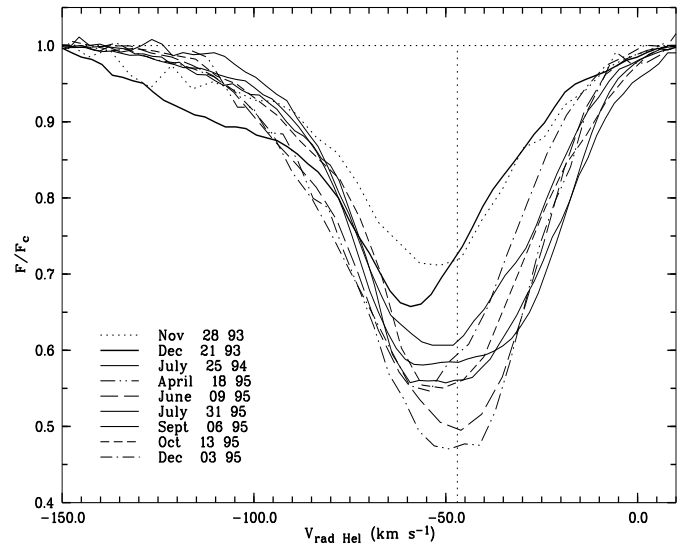


**Fig. 5.** Profile changes of the subordinate Fe I 5572.841 Å line caused by atmospheric pulsation. The dotted vertical line is drawn at the stellar center-of-mass velocity of -47 km s<sup>-1</sup>

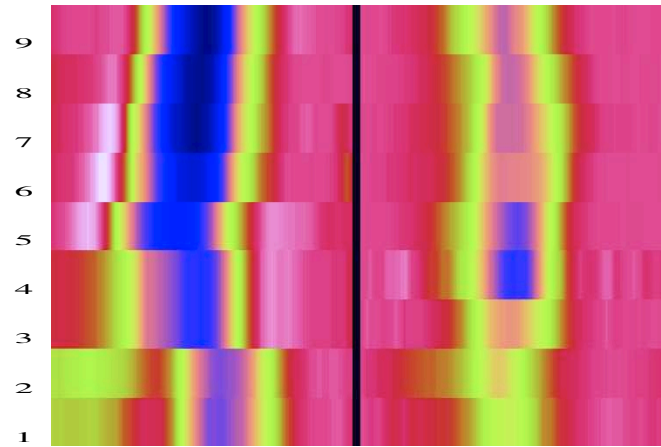


**Fig. 6.** Grayscale sequence of H $\alpha$  (panel left) and of Fe I 5572 spanning a period of 24 months. The heliocentric radial velocity scale on the abscissa ranges from -150 to 50 km s<sup>-1</sup> in both panels. Notice the striking opposite displacement of both line cores in strips 5-9 which belong to a single pulsation period. Notice that the H $\alpha$  profile of strip 4 is lacking (see text)

the same pulsation cycle. It is however questionable whether the three UES spectra (strips 2, 3 and 4) belong to the same pulsation cycle because they have been obtained by seven and nine months apart, respectively, whereas the photometric pulsation period amounts only to 298.5 days, as was determined by Zsoldos & Percy (1991) from data collected between 1963-72 and 1978-89.

Notice the similarity between the line shape of Nov. and Dec. '93 from SAO and UES (strips 1 and 2). By coincidence, both spectra have been obtained with only 24 days in between. Nevertheless, the Fe I line core displays an intensity increase of

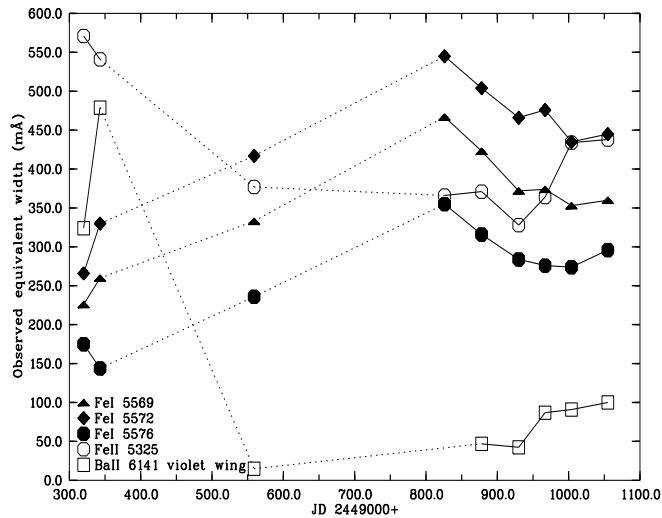


**Fig. 7.** The pulsation modifies the iron ionization equilibrium which causes opposite changes of the equivalent width values of neutral and ionic absorption lines. These changes correspond to a decrease of  $T_{\text{eff}}$  by  $\sim 400$  K between April and Dec. '95

as much as 5 percent. Such rapid intensity changes indicate that the three UES spectra are not reflecting a smooth variation of the atmospheric conditions during the 16 months they overspan. We remark however that the majority of the neutral lines appear to intensify nearly linearly during that period, combined with a redward displacement of the line bisector.

In Fig. 7 we show the changes of the equivalent line widths resulting from the atmospheric pulsation of  $\rho$  Cas. The three neutral iron lines at 5569 Å, 5572 Å and 5576 Å belong to the same multiplet (686), having  $\log(gf)$ -values of -0.54, -0.31 and -1.0, resp. (Table 1). The observed increases of  $W_{\text{eq}}$  by about 200 mÅ between Dec. '93 and April '95 correspond with a decrease of  $T_{\text{eff}}$  by 750 K, from 7250 K to 6500 K (Sect. 3.1). The subsequent decrease of  $W_{\text{eq}}$  by about 100 mÅ, measured from the five SAO spectra between June and Dec. '95 correspond therefore with an increase of  $T_{\text{eff}}$  by 400 K at most. This relatively small change of  $T_{\text{eff}}$ , covering almost half of the pulsation period, is in reasonable agreement with a range in  $T_{\text{eff}}$  of  $200 \pm 100$  K which was determined for the pulsation in Jan.-July '70 (Lobel et al. 1994, see their Fig. 1). The increase from 7050 K to 7250 K was also derived from varying  $W_{\text{eq}}$  values, corresponding with a decrease by 60% of the weakest Fe I lines and about 40% for the strongest, whereas the  $W_{\text{eq}}$  values of the Fe II lines increased. Also in the present data of Table 1 the majority of the neutral iron lines increases by about 100-200 mÅ, while most of the Fe II lines (i.e. at 5325 Å, 5316 Å and 5425 Å) weaken between Dec. '93 and April '95 (UES data). These changes of  $W_{\text{eq}}$  for the Fe II 5325 Å line have also been measured in the 5 SAO spectra and the complete sequence is plotted in Fig. 7.

The opposite variation of the neutral and ionic lines results from a displacement of the ionization equilibrium during the atmospheric pulsations. The changes of  $T_{\text{eff}}$  vary around

$T_{\text{eff}} \approx 7000$  K which changes the thermal conditions in the line formation region. The bulk of the medium-strong lines measured by us emerges from layers with  $\tau_{\text{Ross}} \leq 1$  covering an atmospheric extension of  $\sim 40 R_{\odot}$ . Although the computed  $W_{\text{eq}}$  values depend of four model parameters ( $T_{\text{eff}}$ ,  $\log g$ ,  $\zeta_{\mu}$  and  $\Delta \log Z$ ), we find that these changes are most sensitive to the alterations of  $T_{\text{eff}}$  alone. This dependence has also been considered by Gray (1992, Fig. 13.6). For a lowering of  $T_{\text{eff}}$  by 500 K the width of an Fe II line decreases from a maximum value around 7000 K, whereas the Fe I lines grow steeply over that range. Therefore, the modifying particle density causes a change of the line strength which can be computed from Eqns.(13.21) of Gray. These calculated changes correspond very well with the changes of  $W_{\text{eq}}$  obtained from our best model fits (by utilizing the SYNSPEC code) presented in Table 1 and Fig. 7.

Notice that the profile changes in Fig. 5 do not result from pressure effects in the line formation region. This is evidenced from the selected model atmospheres of which the changes in the pressure gradients remain minor for a relatively small decline of  $\log g$  from 1.0 to 0.5. Therefore, the triangular line shapes of Nov. and Dec. '93 are not caused by pressure broadening effects. In Sect. 3.6 we will demonstrate that this peculiar shape of the profiles is linked with the discontinuously extended violet wing of the line, which show up during the phase of highest effective temperature in the pulsation cycle.

### 3.3. The radial velocity curves of 1993-95

In Fig. 8 we show the heliocentric radial velocity curve ( $V_{\text{rad}}$ ), measured from Fe I 5572 Å, Sc II 5641 Å and Y II 4900 Å. These lines are not blended which we have verified by means of a synthetic spectrum modeling. However, we find that several other lines which were selected in the spectra of '70 ought to be rejected for velocity measurements because of hidden line blends (i.e. Y II 4854 Å). The profiles of the Sc II and Y II line are provided in Figs. 9 and 10, because their excitation energy ( $\sim 1$  eV) is smaller than for the Fe I line. Notice that the Sc II profile displays the broadening and narrowing with time at the longwave side of the line core, similar as is observed in Fig. 5 for the Fe I line. The flat-topped shape of the Y II line is observed among many other low energy lines in the spectra. These line cores are filled in by weak emission from cool and diffuse shells near  $\rho$  Cas (Lobel & de Jager 1997).

We have measured the  $V_{\text{rad}}$  values by means of a least-square fit of a Gauss function onto the observed line body. The values plotted in Fig. 8 are thus measured from the line bisector of the Gauss fit at half intensity. When taking the spectral resolution into account and the accuracy of the wavelength calibration criterion (or the dispersion curves), together with our method of measuring these single-run spectra, we estimate the accuracy of the  $V_{\text{rad}}$  quantities listed in Table 3 around  $\pm 2$  km s $^{-1}$  at best.

Fig. 11 shows the profile changes of H $\alpha$ , and the  $V_{\text{rad}}$ -curve is also given in Fig. 8. Notice the large amplitude of  $\sim 35$  km s $^{-1}$  when compared to that of the three metallic lines of about 10 to 15 km s $^{-1}$ . An amplitude that large has also been reported by Sheffer & Lambert (S&L 1986) for the H I 8750 Å line,

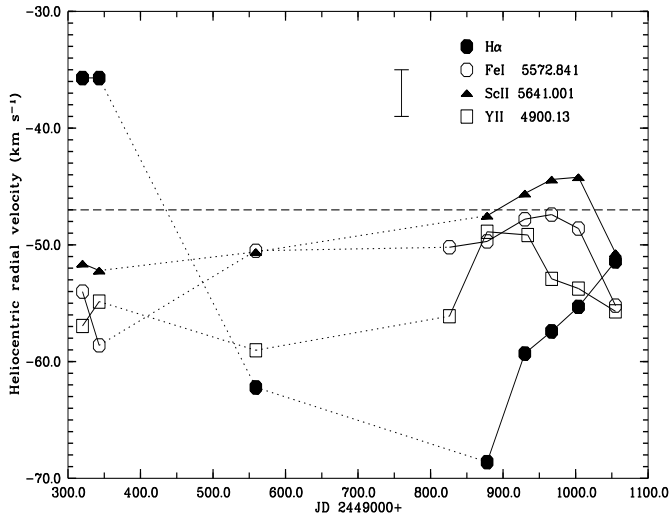


**Fig. 8.** Heliocentric radial velocity changes of the H $\alpha$  line core and of three metallic lines ( $\chi_{\text{low}} < 3.4$  eV) with respect to the stellar velocity (dashed drawn line)

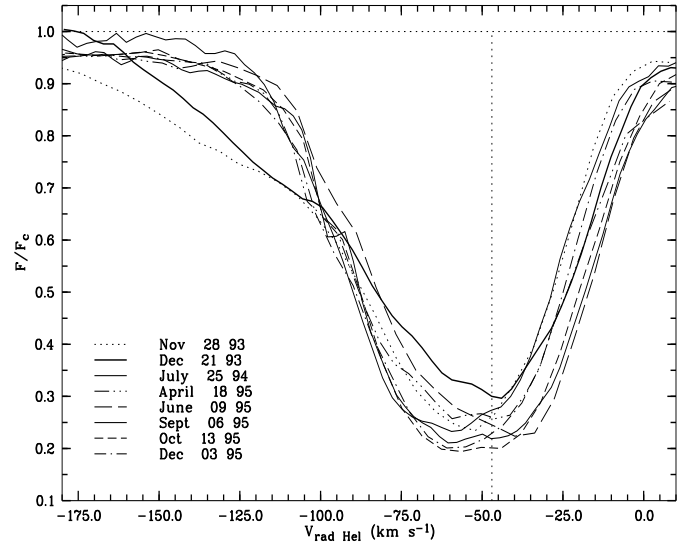


**Fig. 10.** The flat-topped line shape of Y II 4900 indicates a permanent filling-in by emission of very low excitation energy

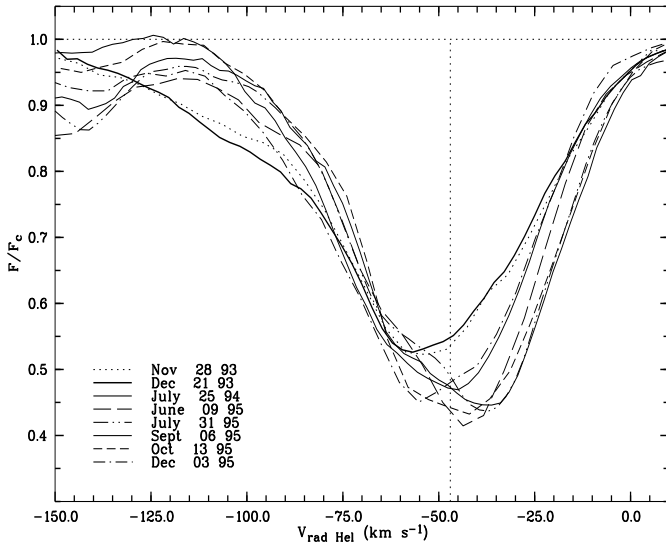


**Fig. 9.** The profile changes of Sc II 5641 correspond to these of Fe I 5572. The line cores broaden and narrow at the longwave side with the pulsations of  $\rho$  Cas

ranging from  $-35$  to  $-60$   $\text{km s}^{-1}$  over a period of about 300 days in 1982-83 (see their Fig. 1). However, we can not confirm the amplitude for the Fe I line at  $6400 \text{ \AA}$  exceeding a range of  $40$   $\text{km s}^{-1}$ . Also the low excitation line of Ba II at  $6141 \text{ \AA}$  turned out to be unfit for velocity measurements in our spectra, which we will discuss in Sect. 3.5.

We find that the velocity variations of all unblended metallic absorption lines having  $1 \text{ eV} < \chi_{\text{low}} < 5 \text{ eV}$  remained below  $15$   $\text{km s}^{-1}$  during the period of our observations. The latter value for these absorptions, which are formed in the middle to upper atmospheric layers, compares to a value of  $14$   $\text{km s}^{-1}$  which

**Table 3.** Heliocentric radial velocity values in  $\text{km s}^{-1}$  of three metallic absorption lines and of the H $\alpha$  line core between Nov. '93 and Dec. '95

Obs. date	No.	H $\alpha$	Fe I	Sc II	Y II
$\lambda_0$ ( $\text{\AA}$ )		6562.817	5572.841	5641.001	4900.13
Multiplet		(1)	(686)	(29)	(22)
$\chi_{\text{low}}$ (eV)		10.15	3.40	1.49	1.03
$\chi_{\text{up}}$		12.04	5.60	3.88	3.55
Nov. 28 1993	1	-35.5	-54.0	-51.6	-57.0
Dec. 21 1993	2	-35.5	-58.5	-52.2	-55.0
July 25 1994	3	-62.0	-50.5	-50.6	-59.0
April 18 1995	4	-	-50.0	-	-56.0
June 09 1995	5	-68.5	-49.5	-47.5	-49.0
July 31 1995	6	-59.0	-48.0	-45.6	-49.0
Sept. 06 1995	7	-57.5	-47.5	-44.5	-53.0
Oct. 13 1995	8	-55.5	-48.5	-44.0	-53.5
Dec. 03 1995	9	-51.5	-55.0	-51.0	-55.5

was given by S&L for the high excitation line of N I  $8703 \text{ \AA}$  in 1980-82. As this line is having  $\chi_{\text{low}}=10.3$  eV, it is formed deep in the photosphere and we conclude from the comparable ranges of our measurements of lines which are formed at higher altitudes, that we are unable to detect from the metallic lines an effect of velocity stratification of the atmosphere of  $\rho$  Cas.

### 3.4. Variability of H $\alpha$

Contrariwise, the  $V_{\text{rad}}$  curve of H $\alpha$  appears in anti-phase with the metallic lines in Fig. 8. This behavior can also be observed in the left panel of Fig. 6 (notice that strip 4 is lacking here because the UES spectrum of April '95 was overexposed above  $5600 \text{ \AA}$ ). Since the H $\alpha$  line core emerges in average from higher

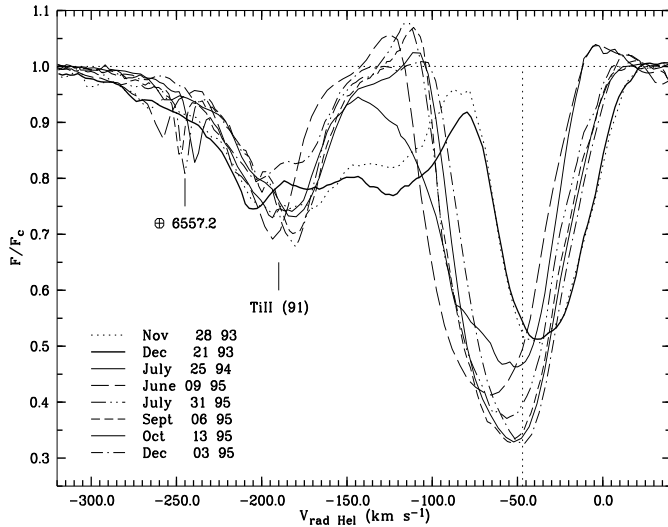


**Fig. 11.** In contrast to the metallic lines, the  $H\alpha$  line core intensifies steadily over 24 months, while the line flanks turn mutually into emission. Notice the tremendous changes in the horizontally far blueward extended line wing over a period of only 24 days (Nov. 28-Dec. 21 '93), whereas the line core remains static

atmospherical layers than the  $\text{Fe I } 5572 \text{ \AA}$  line ( $\chi_{\text{low}} \approx 3.40 \text{ eV}$ ) the opposite Doppler displacements of both centroids might reflect a stratification of their mean formation regions. This may indicate that the upper atmospherical portions are loosely coupled to the deeper layers where the continuum radiation forms, resulting in a velocity curve of  $H\alpha$  lagging behind motions at the base of the atmosphere.

However, we emphasize that the  $H\alpha$  profile is certainly filled in by emission, which affects the  $V_{\text{rad}}$  values measured by us. Sargent (1961) has remarked that the Balmer lines of  $\rho$  Cas were by a factor 10 weaker in 1956-60 than in normal F8 supergiants, which could be caused by filling-in by emission. A contribution of emission is evidenced from the emission humps on either or both sides of the absorption core in Fig. 11. These emissions are also visible in the left panel of Fig. 6 by the white stripes to the outer left of the strips 5, 6, 7 and 8. These cover a period of a least 5 months, where the emission reaches a maximum of 8 percent above the continuum level in July '95. During that period when the line core is shifted most shortward, the prominent emission hump at the longwave side (strips 3 and 4) has completely disappeared. The presence of these emissions appears to be linked with the Doppler displacement of the absorption line core with the pulsation, which indicates a partial filling-in of the line wings. Also the  $H\alpha$  profiles published by Arellano Ferro (1985) displayed prominent emissions in the red flank between May and June '81. We remark further that Mallik & Mallik (1988) have attributed such profile shapes of  $H\alpha$  in G and K supergiants to non-LTE effects in a moving chromosphere by including the effects of hydrogen ionization.

Fig. 12 displays the  $H\alpha$  profile of Nov. 30 1991 in the velocity scale, as was obtained and calibrated for the heliocentric

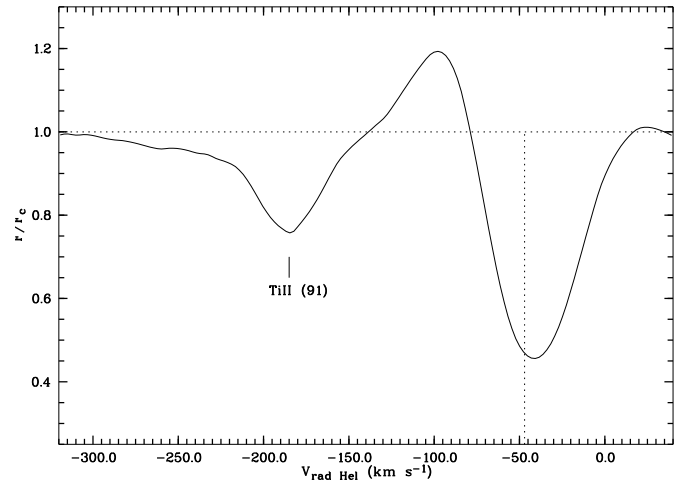


**Fig. 12.** The  $H\alpha$  profile of Nov. 30 1991. The violet line flank is distorted by very intense emission when the red line wing is shifted most longward

wavelength by Dr. Stahl (priv. comm.). This profile is exceptional because of the striking emission peak in the blue flank, almost 20 percent above the continuum level. Nevertheless, we perceive that the intensity of the line core of 0.45 remains comparable with that observed in June '95, when both emission peaks appear much weaker.

The metallic lines broaden and deepen between Nov. '93 and April '95. Thereafter, they weaken and narrow again, reaching a maximum  $V_{\text{rad}}$  value around Sept. 6 '95. The lines are returning shortward since then. In contrast, the  $H\alpha$  line core exhibits an opposite evolution and it has steadily intensified since Nov '93 by about 20 percent over the last two years. Our observations show in any case that the  $H\alpha$  variability occurs on a time scale much longer than that of the metallic absorption lines which are formed deeper. This might reflect a stratification of the very extended atmosphere.

We find from the atmospherical models, determined from our observations by the method of spectral diagnostics in Sect. 3.1, that hydrogen is partially ionized over the complete atmospherical portion where  $-5 < \log(\tau_{\text{Ross}}) < 0$  and  $4000 \text{ K} < T < 8000 \text{ K}$ . As the absorption core of  $H\alpha$  forms over that region we expect that its central intensity changes are strongly sensitive to displacements of the hydrogen ionization equilibrium with the altering atmospherical circumstances during the pulsations. However, our theoretical profile calculations in LTE, utilizing these Kurucz models, revealed that the line core is always saturated with a central intensity near 0.2. This provides another indication that the observed profile must be distorted by emission contributions, possibly from a weak and unsteady quasi-chromosphere due to a field of shock waves (de Jager et al. 1997). They show from non-LTE calculations that continuous trains of weak atmospherical shocks, in association with the observed variation of  $T_{\text{eff}}$ , can reproduce aspects of the variable emission in  $H\alpha$ . Nevertheless, we remark that the prominent emission peaks in  $H\alpha$  stand at variance with the absence of any

clear contribution by emission in the  $H\beta$  profiles during the period of our observations and also in the spectra of '70 (Gesicki, priv. comm.). The absence of any clear emission in the Mg II 2800 Å resonance doublet of the *IUE* spectra of 1979-81 also indicates an hypothetical chromosphere which is variable in time (Sect. 4).

### 3.5. Two types of absorption line splitting

The splitting of the metallic absorption line cores in the spectra of  $\rho$  Cas has often been discussed in the literature. Their appearance is linked with very low excitation energies and we observe them in our spectra for the multiplets (1), (15), (16), (36) and (37) of Fe I, covering the wavelength range of our spectra. For a complete list of multiplets eligible for the core splitting (for lines having  $\chi_{\text{up}} < 3$  eV) we refer to Table 2 of Sargent (1961). We find that the doubling occurs for neutral and ionic metallic lines having  $\chi_{\text{low}} \leq 1.6$  eV. It is caused by a narrow emission reversal which intrudes an absorption line core. Therefore, the splitting is most obvious in very broad absorption lines, preferably having deep and saturated line cores. The superposition of a static emission line onto a Doppler displacing absorption line of varying strength causes the resulting profile to split cyclically (some examples are provided in Lobel & de Jager 1997). When the absorption line remains broad enough during the pulsation, the resulting profile appears permanently splitted. A plain example of the latter profiles observed by us is the Ba II 6141.321 Å resonance line ( $\chi_{\text{low}} = 0.7$  eV) shown in Fig. 13. Its grayscale sequence is also provided in the right panel of Fig. 14. Obviously, the central emission peak remains static, while the absorption flanks are cyclically displaced with time. Notice the shortward shifts of those flanks in the five SAO spectra (strips 5 to 9), which are also observed in the broad Y II 4900 Å line (panel right) and the slender Fe I 5572 Å line profile of Fig. 6 (panel left). The Doppler shifts of the underlying absorption line cause the opposite intensity changes of the apparent absorption dips on either side of the central emission reversal. We refer to Fig. 9 of Gesicki (1992) for a sequence of profiles from another resonance line of Ba II 4934 Å, obtained in 1969-70.

The photospheric absorption line and the circumstellar emission line which composes a splitted profile of low excitation energy originate from the same atomic/ionic transition. However, we have detected the occurrence of a different sort of line splitting in our spectra. The Doppler displacements of a normal absorption line in the neighborhood of a prominent emission line *emerging from a different transition* causes a similar core splitting. The evolution of such resulting 'complex' is shown in Fig. 15. The absorption line core of Fe I 6400.000 Å emerges from multiplet (816) and broadens longward (similar as Fe I 5572 Å in Fig. 5). But the red wing of that line is covered by the permanent emission line of Fe I 6400.314 Å originating from the 13th multiplet. The longward extension of the red absorption wing with time causes this static emission line to gradually fill in the intensifying absorption line, which results in an 'apparent' core splitting between June and July '95. In the following months the red flank of the underlying absorption

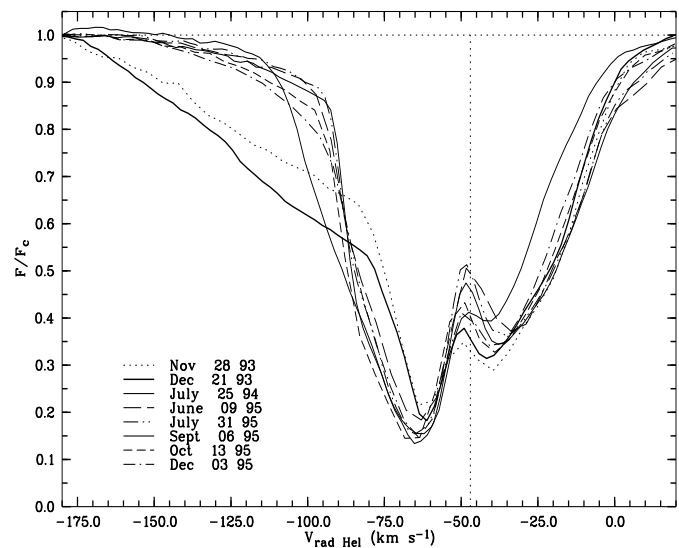


**Fig. 13.** Profile changes of the splitted Ba II 6141.321 Å line of multiplet (2). The central emission reversal near the systemic velocity emerges from the cool static envelope around  $\rho$  Cas. Notice the very far extended violet line wings in the phase of maximum  $T_{\text{eff}}$  (Nov.-Dec. '93)

line fades and the permanent emission line raises again the red wing of the resulting profile. Clearly, this phenomenon should be distinguished from the 'genuine' core splitting commonly observed in the low excitation lines. Both types of core splitting are rapidly confused which results from the tremendously crowded and variable absorption spectrum overlaid with the static emission line spectrum. We conclude that the 6400 Å complex of Fe I lines is clearly unfit for reliable measurements of the radial velocity curve. The splitted profiles of this complex were also presented for Oct. '85 to May '88 and for Sept. '90 and Feb. '91 in Figs. 1 & 2 of Petrov & Herbig (1992). An unsplit profile of Aug. '77 was given in Lambert & Luck (1978) which resembles our line shapes of Sept.-Dec. '95. Another example resulting from this type of 'false' line splitting is provided in Lobel & de Jager (1997) for which the complex is composed by the absorption line Fe I 6358.631 Å and another emission line Fe I 6358.692 Å from the 13th multiplet.

### 3.6. The wind variability and a determination of the mass-loss rate

A most remarkable feature in our spectra is the development of very far extended violet wings around the phase of maximum effective temperature. The resulting profile becomes very asymmetric and these shortward extensions appear in every photospherical absorption line having  $0 \text{ eV} < \chi_{\text{low}} < 10$  eV, irrespective of its oscillator strength. In Nov. and Dec. '93 the wings even display a nearly discontinuous bend in the profile. This phenomenon is obvious for the splitted Ba II resonance line of Fig. 13, but it shows up equally clear for non-resonance lines with either single (i.e. Fe II lines having  $\chi_{\text{low}} > 5$  eV) or splitted cores

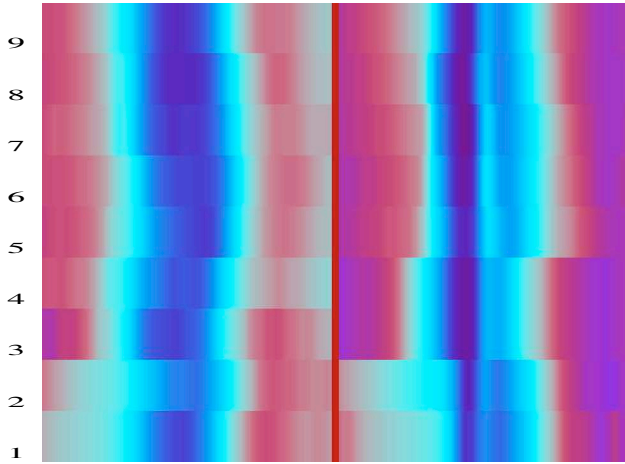


**Fig. 14.** The grayscale sequence of Y II 4900 (panel left) and of Ba II 6141 (panel right). The scale on the abscissas is the same as in Fig. 6. Notice in both lines the red- and blueward shift of the line flanks (bright) over strips 4-9. These lines of low excitation energy ( $\chi_{\text{low}} < 1$  eV) display a very far extended (discontinuous) violet wing in the phase of highest  $T_{\text{eff}}$  (strips 1 and 2) emerging from the supersonic wind. These wings are developing again since April '95

(like the Fe I lines of multiplet (15) having  $\chi_{\text{low}} \simeq 1$  eV). The extended wings retreat in July '94 and are absent in April '95 when  $T_{\text{eff}}=6500$  K and the line profiles become almost symmetric (Figs. 1 & 9). The effective temperature has increased since then and the violet wings are developing again as is visible in Fig. 13 for the Ba II line.

The effect shows also in H $\alpha$  (Fig. 11). Notice the almost horizontal extension in the violet wing of the H $\alpha$  profile of Nov. and Dec. '93 when the line core depression is weakest. An upper radial velocity value for this extension could however not be measured because the violet edge merges with the Ti II line to the left. Nevertheless, the highest velocities which can be ascribed to H $\alpha$  exceed a value of  $150 \text{ km s}^{-1}$ , which seems also present in the simultaneous profiles of H $\beta$ . After Dec. '93 these absorptions fade completely and the blue line flank turns in emission.

We have found that the energy in these discontinuous absorption wings can be measured separately from the line core. This is accomplished by fitting two Gaussians simultaneously onto the line wing and the line core. The fit then optimizes the line intensities and widths by means of a least-square method applied to the observed profile. The result for the Fe I 5576 Å line is shown in Fig. 16. The dashed lines are the best Gaussian line fits, whereas the dotted line is the result by subtracting from the observed line shape (thick drawn line). The equivalent width and the FWHM are computed for both line segments. This procedure reveals that the contributions in the violet line flank thus account for the rather triangular shapes of the resulting core profile around the phase of maximum  $T_{\text{eff}}$ . In Fig. 7 the boxes plot the  $W_{\text{eq}}$  values measured by this method for the violet wing of the Ba II 6141 Å line.

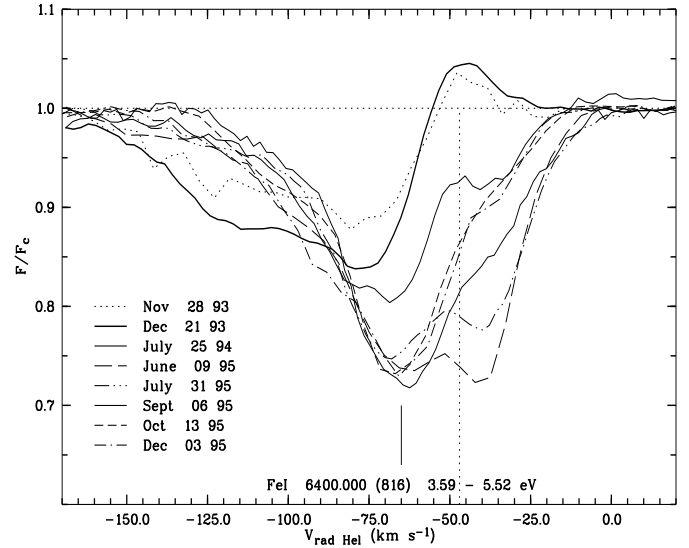


**Fig. 15.** The static emission line Fe I 6400.314 Å from multiplet (13) becomes distorted by variable absorption of Fe I 6400.000 Å from (816) at the left. The complex of lines results in an 'apparent' core splitting in June-July '95

In Fig. 17 we have plotted 9 lines from three different multiplets (168), (686) and (1145/1146) of Fe I, identified in the UES spectrum of Dec. '93. These lines have been retained after checking for the presence of visible or hidden absorption line blending of the observed profile. These multiplets were chosen because of the wide spread in their  $\log(gf)$ -values. For these metallic lines we found that the maximum wind velocities ( $V_{\text{max}}$ ) amount to  $-120 \text{ km s}^{-1}$  with respect to the stellar velocity. Even in the very weak line of (168) the violet wing stretches that far.

We report the finding of a dependency of these  $V_{\text{max}}$  values on the lower excitation energy of the line transition. In Fig. 17 one notices the reduction of  $V_{\text{max}}$  with increasing  $\chi_{\text{low}}$ . The lines of multiplet (1145/6), having  $\chi_{\text{low}} \simeq 4.4$  eV, assume a maximum outflow velocity of nearly  $30 \text{ km s}^{-1}$  smaller than the lines of (168) having  $\chi_{\text{low}} \simeq 2.4$  eV. It results in an increase of the supersonic wind velocity by  $\sim 15 \text{ km s}^{-1}$  per electronvolt decrease.

In Fig. 18 we plot the normalized equivalent width values measured from these violet wings with respect to the  $\log(gf)$ -value of the line transition. When the linear parts of the curve of growth for the three multiplets are matched by shifting them on the  $\log(gf)$  axis, the slope of the linear fit connecting these shifts with respect to their  $\chi_{\text{low}}$  values (in eV) yields the excitation temperature for these shortward displaced absorptions with:

$$\frac{5040}{T_{\text{ex}}} = \frac{\Delta \log(gf)}{\Delta \chi_{\text{low}}} = \frac{3.9}{4.39 - 2.41}, \quad (1)$$

whence, a value for  $T_{\text{ex}}=2560$  K in the wind. The values of the lower energy multiplet levels of Fig. 18 are also given in Table 4.

An estimate of the excitation temperature of these absorptions in the wind of  $\rho$  Cas provides us with an estimate of the

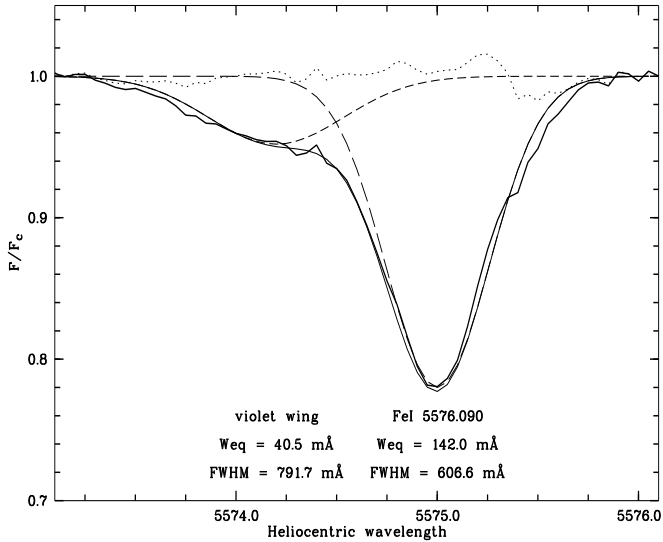


**Fig. 16.** The violet line wing in the phase of maximum  $T_{\text{eff}}$  is separated from the line core by means of simultaneous Gauss fits (dashed lines) on both line segments. The absorptions in the wind account for the triangular shape of the line core in this pulsation phase

related mass-loss rate in this phase of the pulsation when  $T_{\text{eff}}$  is high. In the Kurucz model that we selected for the spectrum of Dec. '93 ( $T_{\text{eff}}=7250$  K,  $\log g=1.0$  and  $\Delta \log Z=0.3$ ) we read a density of  $5 \cdot 10^{-14}$  gr  $\text{cm}^{-3}$  as an upper boundary for the outermost layers of the atmosphere. When combined with the above given maximum wind velocity of  $120 \pm 2$  km  $\text{sec}^{-1}$  and a photospheric radius of  $R_* = 400 \pm 100 R_{\odot}$ , a spherically symmetric mass-loss rate then yields with

$$\dot{M} = 4 \pi R_*^2 \rho V_{\text{max}}, \quad (2)$$

an upper boundary value of  $9.2 \cdot 10^{-5} M_{\odot} y^{-1}$ . The accuracies on the three observables combines to an accuracy for  $\dot{M}$  by a factor of 0.62 or  $\pm 5.7 \cdot 10^{-5} M_{\odot} y^{-1}$ .

We note that the mass-loss rate hence derived from the extended wings of *unsplit* subordinate lines in the optical remains far below the rates recently provided by Gesicki (1992) of  $2 - 4 \cdot 10^{-3} M_{\odot} y^{-1}$  and by Climenhaga et al. (1992) of  $10^{-3} - 10^{-2} M_{\odot} y^{-1}$ . Such extreme values resulted from their modeling of *split* Ba II profiles. We think that these excessive numbers have to be ascribed to the questionable assumption in the wind modeling procedure that the violet 'component' of a splitted absorption line chiefly emerges in a dense 'circumstellar region' surrounding  $\rho$  Cas. In reality, the Ba II resonance lines split because a sharp emission reversal intrudes the broad absorption core of low excitation energy. The emission spectrum emerges from a cool, tenuous and static envelope around the supergiant (Lobel & de Jager 1997). The splitting equally occurs for low excitation non-resonance lines, provided that the absorption core is wide enough to resolve the central emission peak separately.

The absorption in the wind produces an extended discontinuous violet wing in the profile, which develops with the pulsa-

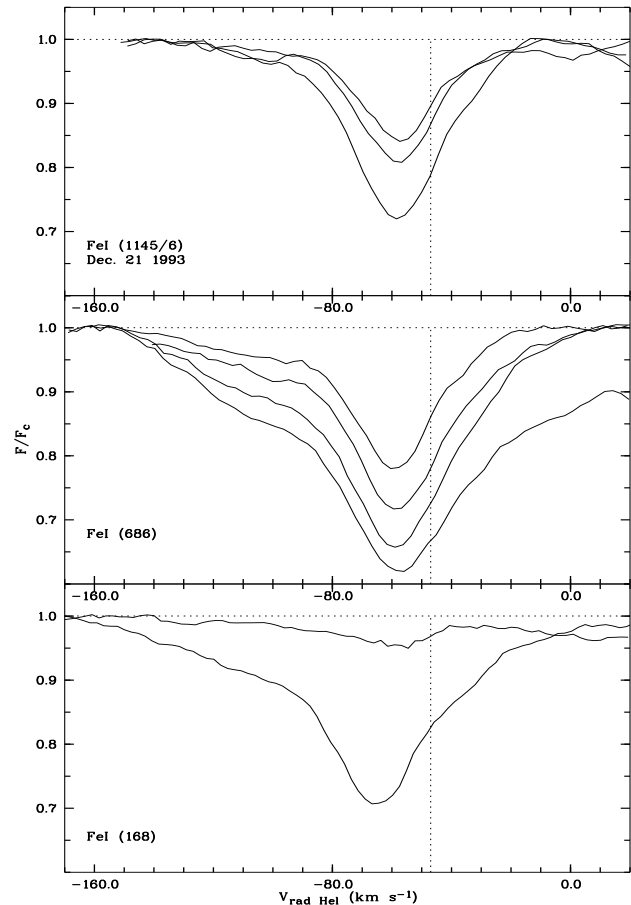


**Fig. 17.** Nine unblended Fe I lines of Dec. 21 '93 from three multiplets given in Table 4. The  $V_{\text{max}}$  values measured in the extended violet wings increase with decreasing lower excitation energy ( $\chi_{\text{low}}$ )

tion of the atmosphere. Such wings appear very pronounced in the spectrum of Nov. and Dec. '93 and they have never been reported before for  $\rho$  Cas. Later in the pulsation cycles one notices that the violet flank of the line core becomes almost vertical and the discontinuous wing disappears. These wings were absent as well in the Ba II profiles of 1969-70 modeled by Gesicki (1992) and of '79 and '81 by Climenhaga et al. (1992).

Our observation with the Westerbork array of  $\rho$  Cas of March 27 1993 detected no radio flux in the 6 cm band. No significant signal was measured at the detection level of 0.2 mJy. The absence of radio emission from  $\rho$  Cas confirms the measurement by Smolinski et al. (1977) of Aug. 1975 at 2.8 cm with ARO. Our upper value of the mass-loss rate of  $9.2 \cdot 10^{-5} M_{\odot} y^{-1}$  for Dec. '93 corresponds with a theoretical flux value at 6 cm of  $S_{\nu} \sim 19$  mJy when computed from the  $S_{\nu}-\dot{M}$  relation of Panagia & Felli (1975) for a source at a distance  $D=3.1$  kpc (Zsoldos & Percy 1991), with a constant outflow velocity of  $184$  km  $\text{s}^{-1}$  (Sect 3.8) and a wind temperature as low as 2500 K. This upper boundary for the expected radio flux level in a pulsation cycle seems more realistic with regard to the absence of a measurable flux in March '93 (we presume being a phase of low  $T_{\text{eff}}$ ) than a

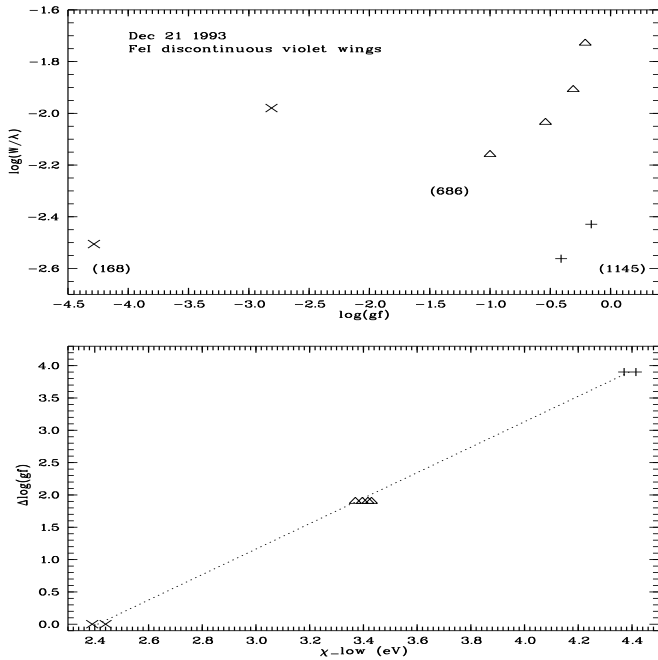


**Fig. 18.** Normalized equivalent width values of the violet wing absorptions against  $\log(gf)$  for 8 Fe I lines. The excitation temperature of the formation region of these extended violet wings is derived from a linear fit (lower panel) over the three selected multiplets (see text)

computed flux being larger by several orders of magnitude obtained with the extreme mass-loss rates of  $10^{-3}$ - $10^{-2} M_{\odot} y^{-1}$  derived for the spectra of 1969-70, 1979 and 1981. Such extreme radio fluxes are not expected because the latter optical spectra did not display the shortward extended discontinuous wing, indicating a phase of low  $T_{\text{eff}}$  with mass-loss rates far below  $9.2 \cdot 10^{-5} M_{\odot} y^{-1}$ . The absence of a measurable radio flux also supports the low temperature we derive in the wind, which is insufficient to ionize hydrogen in order to produce free-free emission.

### 3.7. The formation of far extended violet line wings in the variable wind

The tremendous variability of the violet line wings in the spectra of  $\rho$  Cas may indicate a variable mass-loss rate related to the changes of the atmospherical circumstances, caused by pulsation. The enhancement of these wings does not result from a displacement of the ionization equilibrium with temperature because we observe the increased shortward absorptions simultaneously in neutral and ionic lines. The wing variations could be caused by the changing opacity of a supersonic stellar wind, displaying variable outflow velocities with the varying effective temperature of the hypergiant photosphere. The velocities in the wind assume maximum values when  $T_{\text{eff}}$  is largest and decelerate with descending temperature in the pulsation phase. Therefore, the ‘continuous’ mass-loss rate of  $\rho$  Cas seems to be

surmounted by a ‘pulsational’ contribution determined by these atmospherical oscillations.

An estimate of the extension of the formation region of the enhanced violet wings in the spectrum of Dec. ’93 can be obtained from an estimate of the column density and the particle number density of that line transition in the wind. Since the absorptions in the wing of the 9 Fe I lines of Sect. 3.6 remain small we can approximate their equivalent width values by

$$W_{\text{eq}(\lambda)} \simeq \frac{\sqrt{3}}{2} \frac{\pi e^2}{m_e c^2} N_{\text{col}} f \lambda_0^2, \quad (3)$$

(Unsöld 1955). When the atomic data is combined with the measured  $W_{\text{eq}}$  values it provides the column density  $N_{\text{col}}$  in the wind (Table 4). The number density of the iron particles  $n_{\text{Fe}}$  is obtained from  $n(10^{7.60+0.3})/10^{12} = (\rho/(\mu m_{\text{H}})) 10^{-4.1}$ , where we have assumed  $\mu=1.26$ ,  $[\text{Fe}/\text{H}]=7.60$  (Allen 1973) and  $\rho=5 \cdot 10^{-14} \text{ gr cm}^{-3}$ . When neglecting the fractions from higher ionization stages than Fe II for  $T_{\text{wind}}=2560 \text{ K}$  and adopting the partition function of Fe I given in Gray (1992), we compute from Saha-Boltzmann the particle number density  $n_{\text{Fe I}}^*$  for the lower energy level of these 9 Fe I lines (column 9 of Table 4). The ratio of the column density and the number density then provides an estimate for the extension  $d$  of the region over which the wings of these carefully selected lines form in the wind (column 10). We obtain a mean value of  $1035 R_{\odot}$ , or the wings originate from the wind fraction located about  $2.5 R_*$  above the photospherical radius of  $R_*=400 R_{\odot}$ .

### 3.8. The supersonic wind structure

The structure of the winds of cool supergiants is currently unknown. In order to estimate some characteristics one can however draw a parallel with the winds of hot stars. We assume that the velocity structure of the supersonic wind region can be represented by the common  $\beta$ -power law:

$$v(r) = v_{\infty} (1 - r_0/r)^{\beta} \quad \text{for } r \geq r_s, \quad (4)$$

where  $v_{\infty}$  is the terminal wind velocity and  $\beta$  is a measure of the steepness of the velocity law (Castor et al. 1975). At the sonic point  $r_s$  the wind velocity equals the local speed of sound:  $v(r_s) = v_s$ , whence

$$r_0 = r_s \left( 1 - (v_s/v_{\infty})^{1/\beta} \right). \quad (5)$$

The sonic point connects the sub- and supersonic wind regions and is located close to the stellar surface for supergiant atmospheres. For the extended atmosphere of  $\rho$  Cas we adopt  $r_s=400 R_{\odot}$  where  $v_s=7 \text{ km s}^{-1}$  is a typical value in the outermost layers of the selected atmospherical model with  $T_{\text{eff}}=7250 \text{ K}$ .

In Fig. 19 we plot the supersonic velocity structure for four values of  $\beta$ . The wind accelerates slower for larger values. For this cool supergiant we adopt  $v_{\infty}=1.1 v_{\text{esc}}$ , where the escape velocity is computed from  $(2GM_*(1-\Gamma)/r)^{1/2}$  at the stellar surface for  $M_*=30 M_{\odot}$ , yielding  $v_{\text{esc}}=169 \text{ km s}^{-1}$  and

**Table 4.** Calculated column and particle number densities in the formation region of the shortward extended line wing of 9 unblended Fe I lines (see text)

No.	Fe I	$\lambda_0$ (Å)	$g$	$f$ ( $10^{-2}$ )	$\chi_{\text{low}}$ (eV)	$W_{\text{eq}(\lambda)}$ (mÅ)	$N_{\text{col}}$ ( $10^{13} \text{ cm}^{-2}$ )	$n_{\text{Fe I}}^*$ ( $\text{cm}^{-3}$ )	$d=N_{\text{col}}/n_{\text{Fe I}}^*$ ( $R_{\odot}$ )
1	(686)	5576.090	3	3.3333	3.43	44.1	0.5555	0.2067	386
2	(686)	5572.841	7	9.2711	3.396	68.9	0.3122	0.5544	81
3	(686)	5569.618	5	5.7681	3.417	51.4	0.3748	0.3609	149
4	(686)	5586.763	9	6.8511	3.37	104.4	0.6411	0.8194	112
5	(1146)	5367.476	7	31.9817	4.415	19.5	0.0276	0.005102	778
6	(1145)	5389.46	7	5.5578	4.415	14.8	0.1196	0.005102	3369
7	(1145)	5400.51	9	7.6870	4.371	20.1	0.1170	0.007898	2128
8	(168)	6462.725	9	0.0171	2.44	67.8	123.8592	61.4233	290
9	(168)	6469.12	13	0.0004	2.39	20.2	1574.4434	111.9005	2022

$v_{\infty}=184 \text{ km s}^{-1}$ . Since the luminosity and the stellar mass of  $\rho$  Cas are known only approximately, the dotted lines display the gravitational escape velocities throughout the wind for  $M_*=20, 30$  and  $40 M_{\odot}$ . The Eddington factor  $\Gamma=0.0178$  is adopted from Nieuwenhuijzen & de Jager (1995) for  $30 M_{\odot}$  at an optical depth value of 0.03.

An acceleration of the wind above the sonic point of  $\rho$  Cas, as is modeled by a  $\beta$  law, is supported by our observation that the maximum velocities of the extended violet absorption wings tend to increase with descending excitation energies. It indicates a wind structure speeding up by about  $15 \text{ km s}^{-1}$  per electronvolt decline of the excitation energy (i.e. temperature and density) in the mean formation region of these violet wings. We find that the  $V_{\text{max}}$  values measured from the spectrum of Dec. '93 did not exceed the value of  $130 \text{ km s}^{-1}$  (dashed drawn line). Therefore, the adopted value of  $\beta$  in Eq. (4) is limited by an upper boundary value of unity since the violet wings are formed in the wind within a distance of  $2.5 R_*$  above the photosphere.

We find that for  $\beta = 1$  a particle travels from the sonic point to the distance  $r$  in the supersonic wind over a time:

$$t_s(r) = \frac{r_0}{v_{\infty}} \left( \ln \left( \frac{r - r_0}{r_s - r_0} \right) + \frac{r - r_s}{r_0} \right), \quad (6)$$

which yields  $\sim 3.7$  months for the wind to cross the wing formation region of  $2.5 R_*$ . This is supported by our spectral observations indicating that the far extended violet wings appear for at least a few months in the pulsation cycle. If  $\beta$  assumes values below unity the wind accelerates faster and the travel time reduces. The SAO and UES observations of Nov. 28 and of Dec. 21 '93 cover already 24 days, both showing the extended violet wings.

The density structure of the supersonic wind is

$$\rho(r) = \rho_s (v_s/v_{\infty})(r_s/r)^2 (1 - r_0/r)^{-\beta}. \quad (7)$$

Fig. 19 shows that the decline of the density in the wind steepens with the value of  $\beta$  since one can assume that the equation of mass continuity ( $\dot{M} = 4\pi r^2 \rho v$ ) applies all over the wind. Notice that we have utilized for  $v_s$  in the second factor at the r.h.s. of Eq. (7) the value of  $V_{\text{max}}=120 \text{ km s}^{-1}$  in order to reconcile with the observed mass-loss rate derived in Sect. 3.6. The

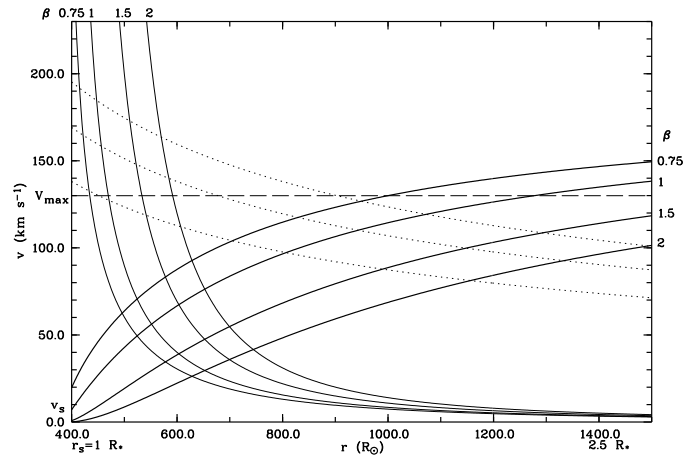


**Fig. 19.** The velocity structure of the supersonic wind region of  $\rho$  Cas for four values of  $\beta$ . The corresponding density structures are given by the thin drawn lines in units of  $\rho_s/500 \simeq 10^{-16} \text{ gr cm}^{-3}$ . The dotted lines are the escape velocities computed in the wind for three values of  $M_*=20, 30$  and  $40 M_{\odot}$

density profile becomes insensitive to changes of  $\beta$  at distances larger than one stellar radius from the photosphere. In that region the wind attains the high velocities which are observed in the variable violet wing extensions of Nov. and Dec. '93. Therefore, the variability of these absorptions can be ascribed to two alternative mechanisms operating in the supersonic wind with the pulsations of the atmosphere of  $\rho$  Cas.

The violet wing variability may be caused solely by cyclic accelerations of the supersonic wind, thus suppressing the value of  $\beta$  below unity during phases of maximum effective temperature. This affects the density only moderately, which maintains the extension of the wing formation region in the wind. In principle, such mechanism could operate without an appreciable change of the mass-loss rate since an increase of the velocity far out in the wind is compensated by an equal but ineffective reduction of the low density gas with a lowering of  $\beta$ . However, a steepening of the supersonic velocity structure with the stellar radiation flux increase would demand for an efficient acceleration

mechanism without strongly disturbing the supersonic density structure. An acceleration of the *subsonic* wind by momentum transfer from the photospheric radiation field seems insufficient to that end because of the small Eddington factor  $\Gamma_F$ . The change of  $\Gamma_F$  under subsonic conditions is computed from

$$\frac{\Delta\Gamma_F}{\Gamma_F} = 4 \frac{\Delta T_{\text{eff}}}{T_{\text{eff}}} + 2 \frac{\Delta R_*}{R_*} + \frac{\Delta\kappa_R}{\kappa_R}. \quad (8)$$

For a change of  $T_{\text{eff}}=7000$  K by about 1000 K due to the pulsation, together with  $\Delta R_*$  of about  $100 R_\odot$  and  $R_*=400 R_\odot$  we find that  $\Delta\Gamma_F \simeq \Gamma_F$ , where the changes of the flux-mean-opacity can be neglected. But in the supersonic wind region the change of the classical Eddington factor has to be multiplied by  $M(k, \alpha, \delta)$  which corrects for the radiation pressure due to lines (Castor et al. 1975). Hence, for constant  $M$  we find  $\Delta\Gamma = \Delta\Gamma_F M \simeq \Gamma_F M = \Gamma$ , which grows in the supersonic wind and which leads to significant adaptations of the momentum balance with the pulsation cycles. We have computed  $M$  for the velocity structure with  $\beta = 1$  and find values increasing from 2.2 at the sonic point to 9.5 near  $2.5 R_*$ . These were obtained by setting  $\alpha=0.66$ ,  $k=0.54$ ,  $\sigma_e=0.34$  and the thermal velocity of hydrogen  $v_{\text{th}}=6.4 \text{ km s}^{-1}$  for  $T_{\text{wind}}=2500$  K. The values of  $\alpha$  and  $k$  (and  $\delta=0.058$ ) were derived from a linear extrapolation to  $T_{\text{eff}}=7000$  K of the tables provided by Shimada et al. (1994). Note that the latter were given for LTE conditions down to a lower boundary of  $T_{\text{eff}}=10000$  K. The high value of  $k$  results from the large number of singly ionized metals. Hence, we find that  $\Gamma$  grows in the supersonic wind to non-negligible values of 0.17 and may vary there by the same amount with the atmospheric pulsations.

Alternatively, the pulsation of the atmosphere may induce very large changes of the mass-loss rate in a cycle (by a factor of 10 say). Since  $\dot{M}$  is proportional to  $\rho$  this strongly changes the density structure of the supersonic wind. Consequently, the extension of the formation region of the violet absorption wings will modify. When assuming that the density roughly scales with this extension (assuming an almost invariable supersonic temperature structure) a decrease of the mass-loss rate by a factor of 10 would squeeze the wing formation region from  $2.5 R_*$  (near maximum  $T_{\text{eff}}$ ) to  $0.25 R_* \simeq 100 R_\odot$  above the sonic point. There, the wind velocities are too small to exceed the thermal velocity in the wing of the absorption lines emerging from the photosphere. When the core profiles become deep and rather symmetric the maximum velocities measured from the violet wings do not exceed about 60 to 70  $\text{km s}^{-1}$ . We note in Fig. 19 that the wind velocity remains below these values within one stellar radius from the sonic point only for values of  $\beta$  exceeding unity. Such large changes of the mass-loss rate can perhaps result from a transfer of momentum at the base of the wind from mechanical sources in the subsonic wind region. An hydrostatic equation including such sources has been investigated by Nieuwenhuijzen & de Jager (1995) for the atmospheres of cool supergiants.

At present it seems too early to decide between these two options because the spectral information is still too sparse. Certainly, a differential study and the theoretical modeling of the

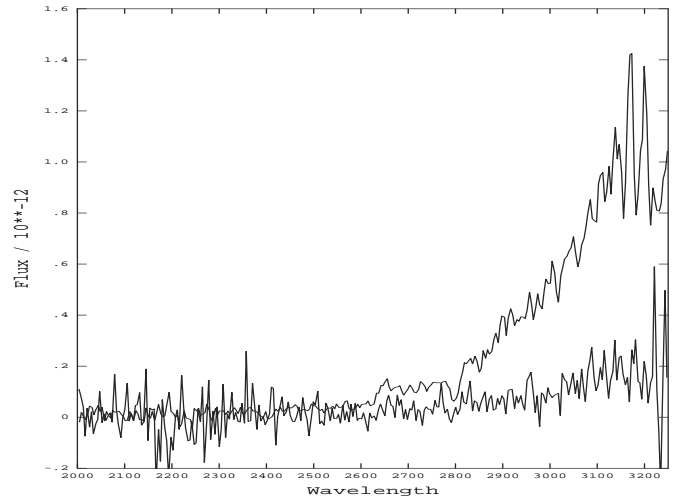


**Fig. 20.** Variability of low-resolution IUE spectra of  $\rho$  Cas. Lower spectrum is no. 03278 and upper no. 03297, revealing tremendous changes of the UV flux in about 26 hours

development and fading of these peculiar violet line wings, discontinuously extending shortward during the phase of maximum effective temperature, can provide a clue. A primal indication may be obtained from measuring changes of the gradient of  $V_{\text{max}}$  values with excitation energy over subsequently obtained spectra in order to check whether or not the wind acceleration is changing during that phase of the pulsation cycle.

#### 4. Variability of the UV spectra of 1979-81

The UV flux of  $\rho$  Cas in Fig. 20 is very small because of the low effective temperature. Most of the spectral features result from the resonance lines of Mg, Fe and Al. For many cool supergiant objects the strong Mg II resonance doublet at  $2800 \text{ \AA}$  appears to be displaced shortward with respect to the stellar velocity, indicating outflow. We have detected very rapid and intense variations of the Balmer continuum flux in the low-resolution IUE spectra of  $\rho$  Cas. In Fig. 20 we plot these spectra of Dec. 26-27 1978, obtained by about 26 hours apart with small aperture. The large intensity change by a factor of 4 or more confirms the short-time variability of the Balmer continuum flux reported by Joshi & Rautela (1978), who indicated an enhancement of the continuum shortward of  $4000 \text{ \AA}$ . They found changes of 0.4 mag. of the flux around  $3400 \text{ \AA}$  on two successive nights of Oct. 2-3 '74. The variation of this emission indicates a burst-like heating mechanism of a weak and temporary chromosphere, although one ought to realize that a suitable source is hard to identify from such limited amount of data.

The changes of the Balmer continuum flux seem to occur independently from the variability of  $H\alpha$ , which was discussed in Sect. 3.4. The latter seems to be linked with the long-term quasi-regular changes of the atmospheric conditions with pulsation as we inferred from optical spectra, whereas the first behaves rather erratic with periods of one day or shorter. The differing

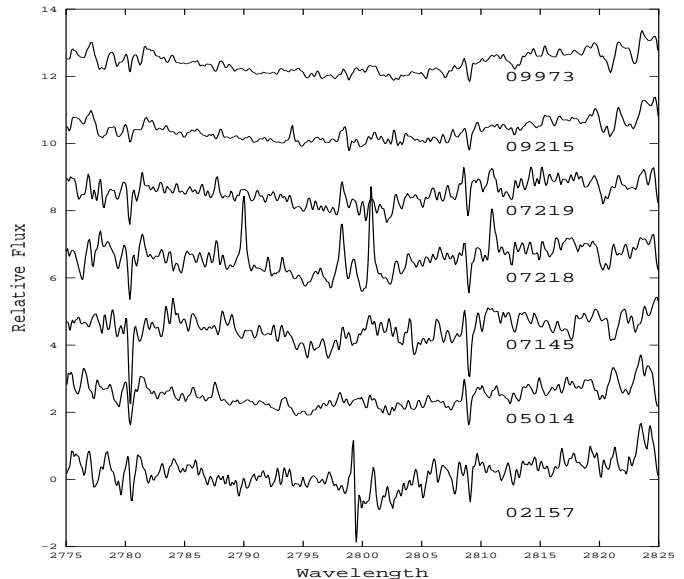
**Table 5.** Dates and hour of observation of reduced *IUE* spectra of  $\rho$  Cas in 1979-81

Image No.	Disp./Apert.	Obs. date	Exposure length (sec.)
LWR03278	LS	Dec. 26 1978 04:35	00190
LWR03297	LS	Dec. 27 1978 06:05	00600
LWR02157	HL	Aug. 23 1978 07:46	01800
LWR05014	HL	Jun. 12 1979 05:09	26820
LWR07145	HL	Mar. 10 1980 07:11	12600
LWR07218	HL	Mar. 17 1980 11:43	10800
LWR07219	HL	Mar. 17 1980 15:12	13200
LWR09215	HL	Nov. 02 1980 21:06	15300
LWR09973	HL	Feb. 21 1981 16:53	28800

origin of the optical and UV flux variations is supported by noting that the time-scale for assuming radiative equilibrium after photo-ionizing hydrogen by UV radiation is much shorter for the atmospheric layers where the  $H\alpha$  absorption core forms, when compared to the period of the Balmer continuum changes. The time  $t_*$  required for establishing radiative equilibrium is  $t_* = 1/n \sum_{i=2}^{\infty} C_{if}$ , where  $C_{if}$  is the photo-recombination probability of level  $i$  and  $n$  the particle number density of hydrogen atoms (Ambartsumyan 1958). When assuming an electron temperature of  $10^4$  K in the photo-ionizing region we can adopt  $\sum_{i=2}^{\infty} C_{if} \sim 3 \cdot 10^{-13}$ , and for a recombination time of  $t_* = 1$  day we find  $n = 3.8 \cdot 10^7 \text{ cm}^{-3}$ , which remains far below the hydrogen particle number density in the photospherical  $H\alpha$  formation region.

In Fig. 21 we show the variability of the Mg II resonance doublet observed in 7 high-dispersion spectra. The observation dates corresponding with the image numbers are given in Table 5. Note that image no. 03297 has been mentioned in Parsons (1980). The doublet profile appears fully in absorption but varies with time. Notice the weakening of the doublet with time where the core absorptions almost fade around Feb. '81 which results from a decrease of  $T_{\text{eff}}$  with the pulsation. We have fitted two of the profiles, collected by about 17 months apart, by using the approximated non-LTE approach of Rybicki (1984). We found that the calculations in pure LTE would underestimate  $T_{\text{eff}}$  by about 200 K. The theoretical profile fits are presented in Fig. 22. The best fit to the observed and smoothed profiles confirms the atmospheric model parameters which we have derived from the optical spectra, in agreement with a variation of the effective temperature by about 750 K.

The phase of minimum effective temperature around Nov. 02 '80, inferred from fitting the weak Mg II doublet, is confirmed by the observation that the  $H\alpha$  core profile of Nov. 06 '80 (Arellano Ferro 1985) becomes deep (near maximum depression) and resembles the deep and symmetric core shape of June 09 '95 (Fig. 11) in the phase of minimum  $T_{\text{eff}}$ , as we have derived from the optical spectra.

**Fig. 21.** Variability of the Mg II resonance doublet from high-resolution *IUE* data between Aug. '78 and Feb. '81. Flux values are normalized and the images are shifted upwards

## 5. Summary and conclusions

We have analyzed 9 optical spectra of  $\rho$  Cas covering a period of 2 years. We find a decrease of  $T_{\text{eff}}$  by 750 K from 7250 K in Dec. '93 to 6500 K in April '95. The values of the stellar model parameters and the temperature range are confirmed by a theoretical modeling of the variability of the Mg II doublet at 2800 Å between Jun. '79 and Nov. '80. The previously reported value of the microturbulence between 10 and 13  $\text{km s}^{-1}$  is confirmed by optimal profile fits to carefully selected metallic absorption lines in our spectra. From these we find a best value for  $v \sin i$  of 25  $\text{km s}^{-1}$ , which limits the stellar rotation period to 809 days for a photospherical radius of 400  $R_{\odot}$ . The time-scale of the profile changes of metallic lines belonging to a single pulsation period, subsequently monitored since April '95, exceeds already 9 months. The intensity and radial velocity changes of the  $H\alpha$  line core appear in anti-phase with a much longer period, which might reflect a velocity stratification of the extended atmosphere of  $\rho$  Cas. The variability of  $H\alpha$ , which is linked with the atmospheric pulsation, is however distorted by a clear filling-in by emission, presumably from a weak and varying chromosphere. These emission contributions stand at variance with the absence of prominent emission in  $H\beta$  and the absence of emission in the UV Mg II resonance doublet of 1979-81. The enormous changes of the Balmer continuum flux observed over a period of 26 hours occur independently from the atmospheric pulsation.

We have found another type of cyclic line splitting for the cores of absorption lines with the pulsation. The line splitting phenomenon for  $\rho$  Cas has commonly been reported for low energy lines and is caused by the superposition of a photospheric broad absorption line and a static emission line from the same

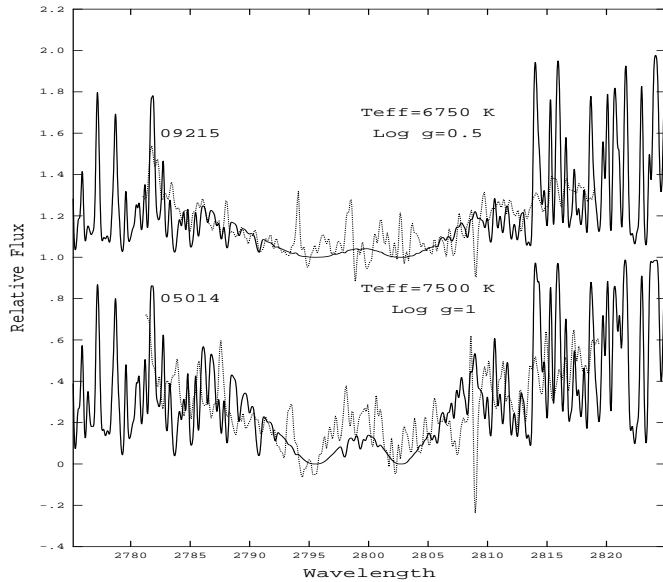


**Fig. 22.** Profile fits of the Mg II doublet using Kurucz atmospheric models. Flux values are normalized and image no. 09215 is shifted upwards. The observed spectra are smoothed with a Gaussian profile of FWHM=0.2 Å

atomic transition, emerging from a cool tenuous shell surrounding  $\rho$  Cas. We find that splitted line cores of  $\rho$  Cas can also be composed of an absorption and an emission line of different atomic transitions. Such a complex of lines is found at 6400 Å where a Doppler displacing photospheric absorption line becomes splitted by the intrusion of a static emission core of the 13th multiplet of Fe I. Therefore, these complexes are unfit for measurements of the radial velocity curve. We could not detect a velocity stratification from unsplit metallic absorption lines with  $1 \text{ eV} < \chi_{\text{low}} < 5 \text{ eV}$  in our sequence of spectra. The amplitude of the latter lines remains below  $15 \text{ km s}^{-1}$ , whereas the H $\alpha$  line core exceeds  $35 \text{ km s}^{-1}$  over the same period.

Our spectra of Dec. and Nov. '93 display the development of very far shortward extended wings in every photospheric absorption line. The spectra correspond to phases near maximum  $T_{\text{eff}}$ , while these extended wings disappear for low  $T_{\text{eff}}$  when the profiles become deep and center almost symmetrically around the stellar velocity. These absorptions are produced in a supersonic wind for which we measure maximum outflow velocities of  $150 \text{ km s}^{-1}$  in H $\alpha$  and velocities up to  $130 \text{ km s}^{-1}$  for metallic lines of very low excitation energy. A multiplet analysis of 9 unblended Fe I lines reveals an excitation temperature of 2560 K in the supersonic wind. It corresponds with an upper value of the mass-loss rate near the phase of maximum  $T_{\text{eff}}$  of  $9.2 \cdot 10^{-5} M_{\odot} \text{ y}^{-1}$ . The latter value would confirm the absence of a radio flux derived by us 9 months earlier for a phase of low  $T_{\text{eff}}$ , linked with smaller mass-loss rates.

We have modeled the velocity structure of the supersonic wind by a  $\beta$ -power law. This is supported by our finding that the maximum velocities of the violet extended wings of Fe I tend to increase by  $\sim 15 \text{ km s}^{-1}$  per electronvolt decline of the exci-

tation energy (i.e. with a lowering of the temperature or density in the supersonic wind). We compute that the mean formation region of these wings is located about  $2.5 R_{*}$  above the upper atmospheric layers, where the sonic point occurs. The latter distance limits  $\beta$  to an upper boundary value of unity during the phase of high  $T_{\text{eff}}$ . The enhancement of the violet wings with the pulsation of the photosphere of  $\rho$  Cas can be ascribed to two alternative mechanisms. Either the supersonic wind is accelerated radiatively with the raise of  $T_{\text{eff}}$  in combination with an almost invariable mass-loss rate which maintains the extent of the wing formation region, or mechanical sources from the subsonic wind region modify the mass-loss rate drastically which alters the violet wing formation region and hence the observable wind velocities. The spectral monitoring program of  $\rho$  Cas presently scheduled at SAO, and additional spectra to be obtained at La Palma, will hopefully shed more light on the wind driving problem for this cool enigmatic object.

*Acknowledgements.* A.L. acknowledges financial support by the Fund for Scientific Research - Flanders (Belgium) in 1995-97. F.M. acknowledges the Russian Science Foundation under the grant N95-02-04276. We sincerely thank Drs. R. Rutten, R. Peletier and N. Walton for coordinating the service observations of  $\rho$  Cas with UES at La Palma in 1993-95. We express our thanks to Dr. O. Stahl for kindly providing the authors with a broad and fully calibrated optical spectrum of 1991. Dr. T. Spoelstra of the NFRA at Westerbork is acknowledged for providing reduced radio measurements in 1993. A.L., G.I. and C.d.J. would like to thank Drs. J.P. De Greve (VUB) and H. Nieuwenhuijzen (SRON) for stimulating discussions. A.M. expresses her sincere thanks to Dr. J.P. De Greve for his hospitality. The authors thank Dr. D. Gillet for useful comments and suggestions to this work.

## References

- Achmad L., de Jager C., Nieuwenhuijzen H., 1991, *A&A* 249, 192  
 Allen C.W., 1973, 'Astrophysical Quantities', The Athlone Press, London  
 Ambartsumyan V., 1958, 'Theoretical Astrophysics', p. 464, Pergamon Press  
 Arellano Ferro A., 1985, *Rev. Mex. Astron.* 11, 113  
 Castor J.L., Abbott D.C., Klein R.I., 1975, *ApJ* 195, 157  
 Climenhaga J.L., Gesicki K., Smolinski J., 1992, p. 82 in 'Instabilities in evolved super- and hypergiants', de Jager C. and Nieuwenhuijzen H. eds., North Holland, Amsterdam  
 de Jager C., 1980, 'The Brightest Stars', Reidel, Dordrecht  
 de Jager C., Lobel A., Israelian G., 1997, *A&A Main Journal*, in press  
 Fokin A.B., Gillet D., Breiffellner M.G., 1996, *A&A* 307, 503  
 Fuhr J.R., Martin G.A., Wiese W.L., 1988, *Journ. of Phys. and Chem. Reference Data*, Vol. 17 Suppl. no. 4, Am. Inst. of Physics, New York  
 Galazutdinov H.A. 1992, Preprint of Special Astrophysical Observatory of Russian Academy of Science  
 Gesicki K., 1992, *A&A* 254, 280  
 Gray D.F., 1992, 'The Observation and Analysis of Stellar Photospheres', Cambridge University Press, Cambridge  
 Joshi S.C., Rautela B.S., 1978, *MNRAS* 183, 55  
 Kurucz R.L., 1991, Harvard-Smithsonian Center for Astrophysics, Preprint Series No. 3181

- Lambert D.L., Luck R.E., 1978, MNRAS 184, 405  
Lobel A., de Jager C., 1997, A&A, submitted to Main Journal  
Lobel A., de Jager C., Nieuwenhuijzen H., Smolinski J., Gesicki K., 1994, A&A 291, 226  
Mallik S.V., Mallik D.C.V., 1988, MNRAS 233, 649  
Musaev F. 1993, Pis'ma v AZh 19, 776  
Nave G., Johansson S., Learner R.C.M., Thorne A.P., Brault J.W., 1994, ApJS 94, 221  
Nichols J.S., Linsky J.L., 1996, AJ 111, 517  
Nieuwenhuijzen H., de Jager C., 1995, A&A 302, 811  
Panagia N., Felli M., 1975, A&A 39, 1  
Parsons S.B., 1980, ApJ 239, 555  
Petrov P.P., Herbig G.H., 1992, ApJ 392, 209  
Rybicki G., 1984, 'Methods of Radiative Transfer', p. 21, Cambridge University Press, Cambridge  
Sargent W.L.W., 1961, ApJ 134, 142  
Sheffer Y., Lambert D.L., 1986, PASP 98, 914  
Shimada M.R., Ito M., Hirata R., Horaguchi T., 1994, in IAU Symp. 162, 'Pulsation, Rotation and Mass-loss in early-Type Stars', ed. Balona L.A., Henrichs H.F. and Le Contel J.M., Kluwer, p. 487  
Smolinski J., Feldman P.A., Higgs L.A., 1977, A&A 60, 277  
Unsöld A., 1955, 'Physik der Sternatmosphären', Springer Verlag, Berlin  
Van den Heuvel E.P.J., 1968, Bull. Astron. Inst. Netherlands 19, 309  
Zsoldos E., Percy J.R., 1991, A&A 246, 441